

Cite this: *RSC Pharm.*, 2024, **1**, 1008

## Multilamellar nanovectors composed of microbial glycolipid–polylysine complexes for drug encapsulation†

Silvia Alonso-de-Castro, <sup>a</sup> Sergio Oliveira Formoso, <sup>a</sup> Chloé Seyrig, <sup>a</sup> Korin Ozkaya, <sup>a</sup> Julien Dumont, <sup>b</sup> Luisa Riancho, <sup>c</sup> Javier Perez, <sup>d</sup> Christophe Hélary, <sup>\*a</sup> and Niki Baccile <sup>\*a</sup>

This study addresses the potential use of single-glucose microbial amphiphiles as phospholipid-free drug carriers. Microbial amphiphiles, also known as biosurfactants, are molecules obtained from the fermentation of bacteria, fungi or yeast and are largely studied for their antimicrobial, cleaning or anti-pollution potential. However, recent understanding of their self-assembly properties combined with their interactions with macromolecules suggests broader potential applications, one being the phospholipid-free formulation of drugs. In this study, we demonstrate that this class of bio-based molecules can be directly used to design colloidally-stable vesicular carriers for hydrophobic drugs, without employing phospholipid supports, and that the actives can be delivered to human cells. In this study, multilamellar wall vesicles (MLWVs) have been synthesised using a microbial glycolipid amphiphile and poly-L-lysine, held together by electrostatic attractive interactions. Curcumin, a highly lipophilic molecule, was used as a natural drug model to evaluate the present colloidal system as a potential nanocarrier. The cell uptake of the curcumin-loaded nanocarriers was significantly higher for HeLa cells (50%) compared to normal human dermal fibroblasts (35%) and THP-1-derived macrophages (20%). The cytotoxic effect of delivered curcumin or other pharmaceuticals (doxorubicin, docetaxel, paclitaxel) was higher in HeLa cells as the cell viability was reduced by 50%.

Received 29th May 2024,  
Accepted 11th September 2024  
DOI: 10.1039/d4pm00163j  
[rsc.li/RSCPharma](http://rsc.li/RSCPharma)

### 1. Introduction

Biological amphiphiles, often referred to as biosurfactants, represent a class of amphiphilic molecules synthesised by microorganisms and have garnered considerable attention for their heightened eco-sustainability.<sup>1</sup> Within the spectrum of the available biosurfactant families, glycolipids emerge as particularly relevant macromolecules. Their relevance stems from their high-throughput production process and wide range of applications, with a focus on their use in the biomedical domain, notably in antibiotic development.<sup>2</sup>

The scientific community has so far dedicated some effort in exploring the anticancer properties of microbial glycolipids (e.g., sophorolipids),<sup>3–5</sup> with an ongoing debate about their effects.<sup>6</sup> Only a little work has described the possibility to develop biosurfactant-based carriers<sup>7</sup> from these molecules. Actually, nanocarriers are predominantly composed of phospholipid liposomes.<sup>8,9</sup> Consequently, a more comprehensive work on the impact of biosurfactants on pre-formed bilayer membranes, their structural intricacies, and the potential to deliver drugs is imperative for the assessment of high-quality lipid-based delivery systems.<sup>10–13</sup>

In recent years, advances in the discovery, understanding and control of the self-assembly properties of microbial glycolipid amphiphiles have created opportunities to formulate phospholipid-free and stimuli-responsive complex colloidal structures exclusively composed of bioamphiphiles.<sup>14,15</sup> Multilamellar wall vesicles (MLWVs), members of the polyelectrolyte–surfactant complex family, are interesting colloidal assemblies with notable relevance in the biomedical field. For instance, MLWVs have been previously employed in gene transfection studies, due to their increased stability compared to single-wall vesicles.<sup>16</sup> Our recent investigations revealed the feasibility of manipulating the attractive electrostatic interactions between the microbial C18:1-

<sup>a</sup>Sorbonne Université, Centre National de la Recherche Scientifique, Laboratoire de Chimie de la Matière Condensée de Paris, LCMCP, 75005 Paris, France.

E-mail: [niki.baccile@sorbonne-universite.fr](mailto:niki.baccile@sorbonne-universite.fr), [christophe.helary@sorbonne-universite.fr](mailto:christophe.helary@sorbonne-universite.fr)

<sup>b</sup>Centre interdisciplinaire de recherche biologique, Collège de France, 75005 Paris, France

<sup>c</sup>Centre de Recherche Institut de la Vision, UMR\_S968 Inserm/UPMC/CHNO des Quinze-Vingts, 75012 Paris, France

<sup>d</sup>Synchrotron Soleil, L'Orme des Merisiers, Saint-Aubin, BP48, 91192 Gif-sur-Yvette Cedex, France

† Electronic supplementary information (ESI) available. See DOI: <https://doi.org/10.1039/d4pm00163j>



*cis* single glucose lipid (G-C18:1, GC, Fig. 1), a type of microbial glycolipid with a remarkable colloidal behaviour,<sup>17</sup> and poly-L-lysine (PLL) during the micelle-to-vesicle phase transition of GC. Through this approach, we demonstrated the formation of colloidally-stable, phospholipid-free MLWVs featuring a lamellar architecture composed of alternating layers of GC and PLL. These MLWVs are prepared *via* a pH-stimulated phase transition in aqueous medium, occurring approximately at pH 7.<sup>18,19</sup> Furthermore, GC presents an interesting asymmetric bolaform structure with a free-standing COOH group, which makes the molecules pH-sensitive with a more complex phase behaviour than classical lipids or surfactants.<sup>15</sup>

Drug delivery systems are advanced technologies designed to facilitate targeting and/or controlled release of active pharmaceutical drugs. These systems address numerous challenges associated with the systemic administration of free pharmacological molecules, thereby enhancing their therapeutic efficacy. This improvement is achieved by mitigating several side effects, modulating solubility-related complexities, enhancing biological stability and optimising clearance while minimising non-specific delivery.<sup>20</sup> Drug delivery systems are often in the form of a drug carrier, serving the dual purpose of specific distribution and protection of the active pharmacological principle from degradation and removal by the reticuloendothelial system (RES).<sup>21</sup> Several examples of such delivery systems have been extensively reported in the literature, highlighting the use of liposomes,<sup>22</sup> synthetic polymers<sup>23</sup> or a combination of both,<sup>24</sup> but also polymeric micelles,<sup>25</sup> peptide-based biomaterials,<sup>26</sup> inorganic nanoparticles,<sup>27</sup> gels<sup>28</sup> and biopolymer/clay hybrids.<sup>29</sup> Notably, liposomes, with their characteristic bilayer assembly resembling native extracellular membranes, ease of preparation, and bio-

compatibility stand out as the most commonly investigated nanocarriers for drug encapsulation.<sup>22</sup> Despite their benefits, phospholipid liposomes face several drawbacks including triggering immune response and RES clearance.<sup>30</sup> Therefore, there is a significant need for new alternatives to engineer novel drug delivery systems that can overcome these issues.

In this context, it is of particular interest to evaluate the performance of engineered MLWVs composed of a (non-acetylated acidic) single-glucose microbial glycolipid and a biocompatible polyelectrolyte as a nanocarrier to deliver hydrophobic and hydrophilic drugs, to reduce their clearance and to increase their bioavailability.<sup>31,32</sup> We present here a study on drug loading, cell delivery and cytotoxicity of MLWVs composed of the microbial single-glucose lipid GC and the biocompatible polyelectrolyte PLL (GCPLL MLWVs). This work has focused on the delivery of curcumin, a natural drug studied in a number of nanoscale carriers,<sup>33</sup> and has been extended to include other commercial drugs, like doxorubicin, docetaxel and paclitaxel. Representative studies were performed on cells with different proliferative abilities: mouse fibroblasts (L929), normal human dermal fibroblasts (NHDF), THP-1-derived macrophages and human cervical carcinoma cells (HeLa).

## 2. Materials and methods

### 2.1. Materials

Microbial glycolipid G-C18:1 ( $M_w = 462 \text{ g mol}^{-1}$ ), abbreviated as GC for naming purposes, is composed of a non-acetylated acidic single  $\beta$ -D-glucose headgroup and a C18:1 fatty acid tail (monounsaturation at positions 9 and 10). The GC glycolipid

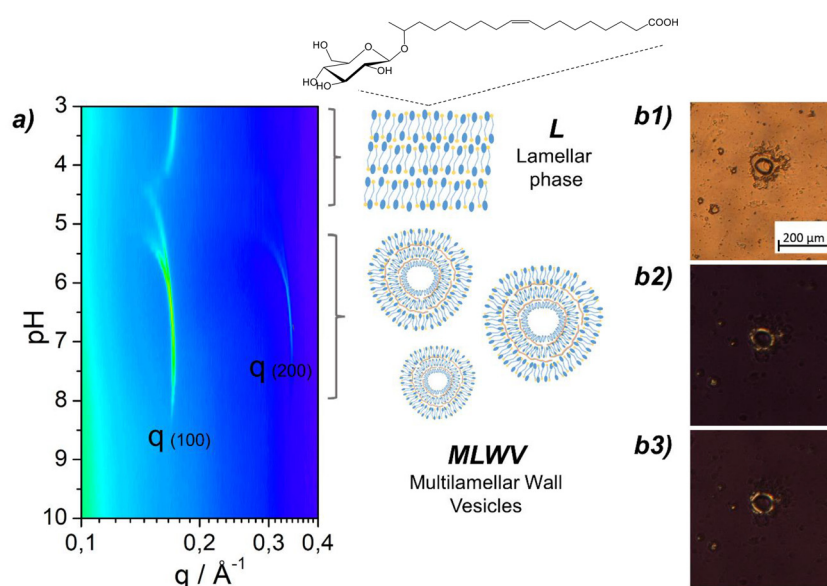


**Fig. 1** (a) pH-resolved *in situ* SAXS (contour plot representation) experiments performed on 2.5 mg mL<sup>-1</sup> GCPLL (GC : PLL = 1 : 1) in DMEM cell culture medium. The schematic representation of the typical lamellar phase (L) and multilamellar wall vesicle assembly (MLWV) is also provided, with the chemical structure of the GC glucolipid. (b1) PLM image of GCPLL MLWVs in DMEM culture medium containing birefringent patterns on the surface evidenced by the rotation of the polarisers from 45°–135° (b2) to 0°–90° (b3).



(lot no. APS F06/F07 Inv96/98/99) was purchased from Amphistar (Gent, Belgium), produced by the Bio Base Europe Pilot Plant (Gent, Belgium), and used without further modification. The molecule was obtained by fermentation from the yeast *Starmerella bambicola ΔugtB1*, according to a previously reported protocol.<sup>34</sup> From the specification sheet provided by the producer, the batch (99.4% dry matter) was composed of 99.5% GC according to HPLC-ELSD chromatography data. NMR analysis of the same compound (different batch) was performed elsewhere.<sup>14</sup> GC molecular purity was higher than 95%. Poly-L-lysine hydrobromide (PLL, 1–5 kDa), curcumin (*Cur*), lipopolysaccharides (LPS), phorbol 12-myristate 13-acetate (PMA), paraformaldehyde (PFA), docetaxel, paclitaxel, and doxorubicin were purchased from Sigma-Aldrich. Lissamine rhodamine B sulfonyl ammonium salt (18 : 1 Liss-Rhod PE, *Rhod*,  $M_w = 1301.7$  g mol<sup>-1</sup>) was purchased from Avanti Polar Lipids. 4',6-Diamidino-2-phenylindole dihydrochloride (DAPI) was purchased from Life Technologies. All chemicals were of reagent grade and were used without further purification unless otherwise specified.

## 2.2. Cell culture

L929 mouse fibroblasts, HeLa human cervical carcinoma cells and normal human dermal fibroblasts (NHDF) were purchased from Merck and cultured in Dulbecco's modified Eagle's medium (DMEM, Sigma) supplemented with 10% foetal bovine serum (FBS, Sigma), 1% penicillin/streptomycin (PS, Sigma) and 1% amphotericin B (Amph-B, Sigma). THP-1 human derived monocytes were purchased from Promocell and cultured in RPMI 1640 medium (Sigma) supplemented with 10% FBS, 1% PS and 1% Amph-B. Cells were then cultured in an incubator at 37 °C with 5% CO<sub>2</sub> under 100% humidity.

## 2.3. Preparation of GCPLL MLWVs

GCPLL MLWVs were prepared according to previously published protocols.<sup>18,19</sup> In brief, stock solutions were prepared by dissolving 5 mg of GC or PLL in 1 mL of DMEM supplemented with 10% FBS. Both solutions were adjusted to pH 10 with small volumes of 1 M NaOH, a step necessary to solubilise GC to a micellar phase, and mixed with PLL in a 1 : 1 volume ratio followed by vortexing. The final concentration of GC and PLL was 2.5 mg mL<sup>-1</sup>. The pH of the mixture was then lowered to 7 with small volumes of 1 M HCl to trigger the formation of MLWVs. At this point, the solution was slightly cloudy, confirming the presence of MLWVs.

## 2.4. Encapsulation of curcumin (*Cur*) in GCPLL MLWVs (GCPLL-*Cur* MLWVs)

A 13.5 mM *Cur* stock solution was prepared in absolute ethanol by thoroughly mixing. After the formation of GCPLL MLWVs in cell culture medium at pH 7, 10 µL of *Cur* solution was added to 1 mL of GCPLL MLWV solution, reaching a final *Cur* concentration of 135 µM. After thorough vortexing, the suspension was centrifuged at 3000 RPM for 5 minutes to collect a pellet of GCPLL-*Cur* MLWVs. The excess, non-encap-

sulated *Cur* present in the supernatant was removed, and the pellet was resuspended in fresh cell culture medium by vortexing.

## 2.5. Encapsulation of doxorubicin, paclitaxel and docetaxel in GCPLL MLWVs

Stock solutions of anticancer drugs were prepared by diluting doxorubicin in DMSO (1 mg mL<sup>-1</sup>), paclitaxel in ethanol (0.1 mg mL<sup>-1</sup>) and docetaxel in ethanol (0.1 mg mL<sup>-1</sup>). In a similar process to that described for the encapsulation of *Cur*, aliquots of 10 µL of each anticancer drug solution were added to 1 mL of GCPLL MLWV solution, followed by the same protocol of centrifugation and resuspension in fresh cell culture medium.

## 2.6. Drug-loading characterisation

The loading capacity (LC%) was calculated as the ratio between the amount of encapsulated curcumin (*Cur*) to the total amount of delivery vehicles (GCPLL MLWVs), and expressed as a percentage (eqn (1)). The encapsulation efficiency (EE%) was calculated by dividing the amount of encapsulated *Cur* by the total amount of *Cur* used during the encapsulation process, and expressed as a percentage (eqn (2)).

$$\text{Loading Capacity (LC\%)} = \frac{\text{mass of encapsulated } \textit{Cur}}{\text{mass of GCPLL}} \times 100 \quad (1)$$

$$\text{Encapsulation Efficiency (EE\%)} = \frac{\text{mass of encapsulated } \textit{Cur}}{\text{mass of loaded } \textit{Cur}} \times 100 \quad (2)$$

## 2.7. Labelling of GCPLL MLWVs and GCPLL-*Cur* MLWVs with rhodamine (GCPLL-*Rhod* MLWVs and GCPLL-*Cur-Rhod* MLWVs)

Both GCPLL MLWVs and GCPLL-*Cur* MLWVs solutions were prepared as previously described. For their labelling using *Rhod*, 10 µL of *Rhod* solution in ethanol (4 mg mL<sup>-1</sup>, 3.08 mM) was added to the corresponding solution so that the GC : *Rhod* molar ratio is 200 : 1. After vortexing, the solution was centrifuged at 3000g for 5 minutes and the pellet was resuspended in fresh cell culture medium. *Rhod* is a standard dye to label lipid bilayers, as its lipid backbone intercalates into this bilayer without any perturbation when the lipid-dye molar ratio is  $\geq 100$ .<sup>35,36</sup>

## 2.8. Small angle X-ray scattering (SAXS)

pH-resolved *in situ* SAXS experiments were performed at room temperature on the Swing beamline at Soleil Synchrotron (Saint-Aubin, France) under proposal no. 20190961. The beam energy was  $E = 12$  keV, the detector was Eiger X 4M, and the sample-to-detector distance was 1.995 m. Silver behenate [ $d(001) = 58.38$  Å] was used as the standard to calibrate the *q*-scale. Raw data collected on the 2D detector were integrated azimuthally using the in-house Foxtrot software provided at the beamline to obtain the typical scattered intensity  $I(q)$ .



profile, with  $q$  being the wavevector [ $q = (4\pi \sin \Phi)/\lambda$ , where  $2\Phi$  is the scattering angle and  $\lambda$  is the wavelength]. Defective pixels and beam stop shadow were systematically masked before azimuthal integration. Absolute intensity units were calibrated by measuring the scattering signal of water ( $I(\text{H}_2\text{O}) = 0.0163 \text{ cm}^{-1}$ ). SAXS profiles were processed with SasView software (v.3.1.2, [sasview.org](http://sasview.org)). The experimental setup was reproduced from previously published work.<sup>18</sup> Briefly, the sample solution (1 mL,  $[\text{CG}] = [\text{PLL}] = 2.5 \text{ mg mL}^{-1}$  in DMEM, pH 11) was maintained in an external beaker under stirring conditions at room temperature ( $23 \pm 2^\circ\text{C}$ ). The solution was continuously flushed through a 1 mm glass capillary using an external peristaltic pump. The pH of the solution in the beaker was changed using an interfaced push syringe, by injecting microliter amounts of a 0.5 M HCl solution. pH was measured using a microelectrode (Mettler-Toledo) and its value was monitored live and manually recorded from the control room. Considering the fast pH change kinetics, the error on the pH value was established as  $\pm 0.1$ .

### 2.9. Polarised light microscopy (PLM)

PLM images were obtained using a Zeiss AxioImager A2 POL optical microscope in transmission mode, equipped with a polarised light source, crossed polarisers, and an AxioCam CDD camera. Images were obtained from a drop of the given sample solution deposited on a glass slide covered with a cover slip.

### 2.10. $^1\text{H}$ solution nuclear magnetic resonance (NMR)

Experiments on the different samples were recorded on an AVANCE III Bruker 300 NMR spectrometer using standard pulse programs and a 5 mm  $^1\text{H}$ -X BBFO probe. The number of transients was 32 with 7.3 s recycling delay, 2.73 s acquisition time, and a receiver gain of 322. Chemical shifts are reported in parts per million ( $\delta$ , ppm) and referenced to 3-(trimethylsilyl)propionic-2,2,3-d4 acid sodium salt (TMSP-d4, Sigma) with a peak at 0 ppm at  $1 \text{ mg mL}^{-1}$  (5.8 mM). Experiments were performed using a 5 mm NMR tube containing 500  $\mu\text{L}$  solution obtained by solubilising the GCPPL MLWVs pellet in MeOD. The pellet was obtained by centrifugation at 3000 RPM for 5 minutes. Signals at  $\delta(\text{PLL}) = 2.8 \text{ ppm}$  ( $t$ ) and  $\delta(\text{GC}) = 2.25 \text{ ppm}$  ( $t$ ) were used for calculations. All samples were prepared using this protocol and all experiments were performed under the same conditions unless otherwise specified. Results and figures are shown in the ESI (pages S2–S5†).

### 2.11. UV-visible spectrometry

UV-visible absorbance spectra of curcumin solutions were collected using a Uvicon spectrometer. Spectra were recorded by measuring the absorbance of curcumin at wavelengths in the range of 190–700 nm.

### 2.12. Cell viability assay

Cell viability experiments were performed with L929 to determine the optimal GCPPL MLWV concentration. Cells were seeded on 24-well plates at a density of  $5 \times 10^4$  cells per mL and cultivated for 24 hours. The following day, GCPPL MLWVs

solutions with concentrations up to  $122 \text{ }\mu\text{g mL}^{-1}$  were added and cells were cultivated for an additional 24 hour period. Furthermore, L929 cultures were exposed to free GC, PLL and DMEM with pH variations. Control samples were cultured in complete medium (supplemented with 10% foetal bovine serum). Cell viability was determined by measuring their metabolic activity using the Alamar Blue Cytotoxicity Assay. Briefly, GCPPL MLWVs were removed from the culture wells and cells were rinsed twice with fresh medium. Then, 300  $\mu\text{L}$  of 0.01% w/v resazurin solution in fresh red phenol-free DMEM medium was added to cells and incubated for 4 hours. The supernatant from each well was then collected, further diluted with 700  $\mu\text{L}$  of fresh red phenol-free medium, and 100  $\mu\text{L}$  was transferred to a 96-well plate to measure absorbance values at  $\lambda = 570 \text{ nm}$  and  $\lambda = 600 \text{ nm}$ . The percentage of resazurin reduction was calculated according to the supplier's instructions and compared to control samples. Then, the effect of GCPPL MLWVs, GCPPL-Cur MLWVs and Cur on the viability was assessed on three different human cell lines (HeLa, NHDF, THP-1). HeLa and NHDF were seeded on 24-well plates at a density of  $5 \times 10^4$  cells per mL for 24 hours prior to the beginning of the experiment. Non-adherent THP-1 cells were seeded at a density of  $5 \times 10^4$  cells per mL in 24-well plates and cultured for 24 hours with serum-free RPMI 1640 medium supplemented with 100  $\text{ng mL}^{-1}$  PMA to differentiate them into adherent macrophage-like cells. Then, differentiation medium was replaced by fresh complete RPMI 1640 medium for an additional 24 hour period. At this point, different concentrations of GCPPL MLWVs were added to the three different cell lines, and following a 24 hour culture time, the cell viability was evaluated using the same Alamar Blue protocol previously described. Finally, cell metabolic activity was compared between samples. The arbitrary value of 100% was given to controls. All experiments were carried out using at least three replicates and the results are expressed as mean values  $\pm$  standard deviation (SD). Statistical significance was analysed by XLSTAT using the Kruskal–Wallis test, with  $p < 0.05$  considered as significant.

### 2.13. Optical fluorescence microscopy

Cells were seeded in 6-well plates at a density of  $5 \times 10^4$  cells per mL and grown for a period of 24 hours under the conditions previously specified. Subsequently, solutions of GCPPL MLWVs, GCPPL-Cur MLWVs, GCPPL-Rhod MLWVs, and GCPPL-Cur-Rhod MLWVs were added to cultured cells at a final concentration of  $100 \text{ }\mu\text{g mL}^{-1}$  and incubated for an additional 24 hour period. Then, after three rinses with PBS, samples were fixed for 1 hour using 4% PFA solution. Following another rinse step with PBS, cells were permeabilised for 15 minutes using a 0.2% (v/v) PBS-Tween solution. Then, 300  $\mu\text{L}$  per well of 1:50 000 DAPI solution were added and cells were incubated for 10 minutes. Finally, after another rinse step, cells were kept at  $4^\circ\text{C}$ , protected from light, until further experimentation. Tagged cells were observed using a ZEISS fluorescence microscope equipped with an AxioCam MRM.



## 2.14. Flow cytometry analysis

Cells were seeded in 6-well plates at a density of  $1 \times 10^5$  cells per well and initially cultured for 24 hours. Then, cells were treated with a  $100 \mu\text{g mL}^{-1}$  MLWV solution and further incubated for another 24 hour period. Cultured cells were detached using trypsin, collected, and centrifuged at 900g for 5 minutes. The cell pellet was resuspended in 1 mL of a 0.5% PFA solution prepared in PBS. Flow cytometry was performed on a CELESTA SORP flow cytometer (BD Biosciences, USA). The acquisition gate was set to record a total of 105 events for each sample.

## 2.15. Confocal laser scanning microscopy

Samples were prepared using the same protocol explained for optical fluorescence microscopy, except that cells were cultured in a Thermo Scientific™ Nunc™ Lab-Tek™ II Chamber Slide with 2 wells for optimal visualisation. Analysis was performed in a spinning disk head X1 (Yokogawa) mounted on a Nikon Eclipse Ti inverted microscope. Cells were observed with a  $60\times/1.4$  Plan Apo objective and a Hamamatsu Orca Flash SC莫斯 camera.

## 3. Results and discussion

### 3.1. GCPPL MLWVs are stable in cell culture medium

Multilamellar wall vesicles composed solely of the glycolipid biosurfactant GC (Fig. 1) and the polyelectrolyte PLL, named GCPPL MLWVs, have been previously reported to self-assemble in mQ-grade water below pH 7.5.<sup>18,19</sup> *In situ* SAXS showed the appearance of two diffraction peaks, corresponding to a lamellar assembly, with period variations in the pH range between 8 and 5. These results were further confirmed by cryo-TEM and PLM, revealing the vesicular shape, the multilamellar structure, and spherulites with a Maltese cross under cross-polarisers. This work complements previous publications and focuses on the characteristics of these self-assembled multilamellar vesicular objects in cell culture medium, fundamental to develop carriers for biological applications. Thus, a similar approach is presented in this work using PLM techniques.

A typical cell culture medium contains a wide variety of compounds such as salts, glucose, and amino acids and is also generally supplemented with proteins coming from foetal bovine serum (FBS). This biochemical complexity may alter the charge, composition and pH range of stability of GCPPL MLWVs. In a process, similar to that described elsewhere,<sup>18,19</sup> the GCPPL MLWVs were prepared by pH modulation in DMEM cell culture medium instead of water. Therefore, the potential interactions with the different biochemical compounds are of great interest. pH-resolved *in situ* synchrotron SAXS was performed on the GCPPL system, varying the pH from alkaline to acidic conditions in DMEM, and the corresponding contour plot between  $q = 0.1$  and  $0.4 \text{ \AA}^{-1}$  is shown in Fig. 1a. At about pH 5, two sharp diffraction peaks appeared, corresponding to the first-order  $q(001) = 0.171 \text{ \AA}^{-1}$  and second-order  $q(002) = 0.341 \text{ \AA}^{-1}$  reflections of the MLWV phase. These peaks evolved during pH decrease and this behaviour is exactly the same as the one previously observed in water.<sup>18,19</sup> Below approximately pH 5, a structural gap appeared

at  $q(001)$ , similar to that previously reported in water systems,<sup>18</sup> revealing the transition between the MLWV and the PLL-free lamellar phase composed of GC only and characterised by a peak at  $q = 0.169 \text{ \AA}^{-1}$ . Therefore, SAXS experiments using synchrotron radiation, performed during the pH-controlled synthesis process, provide the necessary real-time structural information proving the existence of the multilamellar structure of the nanocarriers.

GCPPL MLWVs are birefringent under polarised light.<sup>19</sup> PLM was used to discriminate the shape of the self-assembled entities and to confirm the multilamellar structure in supplemented cell culture media. PLM images were obtained under white (Fig. 1b1) and polarised light (Fig. 1b2 and b3) with polarisers at  $0^\circ$ – $90^\circ$  and  $45^\circ$ – $135^\circ$ , respectively. Additionally, PLM revealed the presence of spherulite structures displaying optical birefringence in the shape of a typical Maltese cross colocalised with the spheroids. These results are in agreement with previously published work<sup>19</sup> and confirm that the interactions between the different biochemical compounds present in the cell culture media do not affect the shape and self-assembly structure of GCPPL colloids in solution.

Previous work has shown that GCPPL MLWVs ( $2.5 \text{ mg mL}^{-1}$ , GC : PLL = 1 : 1) synthesised in water have a broad size distribution centered at about 700 nm.<sup>19</sup> It was demonstrated that classical methods to control their size, like filtration or tip-sonication, work well if needed. However, size control was out of the scope of the present manuscript. GCPPL MLWVs were stable for a pH ranging from 4 to approximately 7.5. The exact extreme pH value was not well defined and possible variations depend on experimental conditions, such as the GC-to-PLL ratio or salt content.<sup>18,19</sup> The present work shows that the use of DMEM cell culture medium did not influence the formation of GCPPL MLWVs. Furthermore, it shows that the domain of pH stability was increased to higher values (approx. pH 8, (Fig. 1)) compared to that found for pure water.<sup>18,19</sup> However, variations in the limits of the pH transition were not unexpected. GCPPL MLWVs are stabilised by attractive electrostatic forces between the negatively-charged GC and the positively-charged PLL. As previously demonstrated by NMR and isothermal titration calorimetry (ITC),<sup>18</sup> the negative and positive charges of these compounds vary with pH and ionic strength. In pure water and in the absence of supplementary salts, the optimal balance of charges for the MLWV phase starts at pH  $\sim$ 7.5. For DMEM cell culture medium, which is rich in salts, it was hypothesised that the optimal charge balance might occur at higher pH values, when part of the negative charges are counterbalanced by the free cations in solution.

Quantitative  $^1\text{H}$  solution NMR, using methanol-*d*4 as the solvent, was employed to determine the content of GC and PLL within the MLWVs using the reference standard TMSP-*d*4.  $^1\text{H}$  NMR spectra (Fig. S1–S4†) showed that GCPPL MLWVs in  $\text{H}_2\text{O}$  (pH = 5.5) contains 70% of the initial amount of GC and 6.5% of initial amount of PLL. However, when GCPPL MLWVs were prepared in DMEM culture medium (pH = 7.4), there was a proportional decrease of both PLL and GC molar ratios, corresponding to 4% and 45%, respectively (Table 1). A reduced content of both GC and PLL in samples prepared in



**Table 1** Quantitative evaluation of GC and PLL in GCPLL MLWVs by  $^1\text{H}$  solution NMR (further explanations on calculations are described in Table S1†). Subscripts: in = initial, f = final

	$C_{\text{in}}$ (mM)		$C_{\text{f}}$ (mM)		$C_{\text{f}}/C_{\text{in}}$ (%)		Molar ratio		Functional group [COOH]/[NH <sub>2</sub> ]
	[GC] <sub>in</sub>	[PLL] <sub>in</sub>	[GC] <sub>f</sub>	[PLL] <sub>f</sub>	GC <sub>f/in</sub>	PLL <sub>f/in</sub>	GC <sub>in</sub> /PLL <sub>in</sub>	GC <sub>f</sub> /PLL <sub>f</sub>	
H <sub>2</sub> O	5.4	1	3.7	0.065	70	6.5	5.4	57	2.8
DMEM	5.4	1	2.4	0.04	45	4	5.4	60	3

DMEM compared to those prepared in water is in agreement with the higher pH values at which MLWVs were formed. As measured by SAXS (Fig. 1a), GCPLL MLWVs were formed in the pH range of 4.5–8. Furthermore, the final molar ratio GC<sub>f</sub>/PLL<sub>f</sub> in H<sub>2</sub>O and DMEM after the preparation of GCPLL MLWVs remained practically constant, at 57 and 60, respectively. The ratio between COOH and NH<sub>2</sub> functional groups, which partially reflects the charge ratio, was 2.8 and 3 for H<sub>2</sub>O and DMEM, respectively. Therefore, both the structural analysis and the composition of the GCPLL MLWVs support their stability at physiological pH in culture medium and their further biological applications.

### 3.2. GCPLL MLWVs are cytocompatible

To the best of our knowledge, the cytocompatibility of GCPLL MLWVs has not been reported. We evaluated their cytocompatibility on the L929 mouse fibroblast cell line by diluting an initial 2.5 mg mL<sup>-1</sup> mixture to obtain different concentrations from 0 to 1 mg mL<sup>-1</sup>. This concentration range was selected to be comparable with other examples on drug delivery systems, such as blank and loaded liposomes.<sup>37–39</sup> All the concentrations referred to the initial quantity employed in the preparation. Besides, the viability of cells was evaluated after incubation with GC and PLL independently. Furthermore, L929 viability was also evaluated with GC-free and PLL-free medium that underwent the same pH changes required to prepare the GCPLL MLWVs. As shown in Fig. 2a, there was no significant cytotoxicity effect observed for GCPLL MLWVs at a concentration of 50  $\mu\text{g mL}^{-1}$ . However, a detrimental effect on L929 metabolic activity was observed for concentrations of 122  $\mu\text{g mL}^{-1}$  and 245  $\mu\text{g mL}^{-1}$ , with a 40% and 80% reduction, respectively. Neither PLL treatment nor pH-dependent medium showed a significant cytotoxic effect under the studied conditions. However, GC treatment had a significant impact on L929 viability. For instance, a GC concentration of 250  $\mu\text{g mL}^{-1}$  resulted in an approximately 20% reduction in cell metabolic activity, and a severe decrease of approximately 90% was observed for GC concentrations higher than 500  $\mu\text{g mL}^{-1}$ .

According to  $^1\text{H}$  solution NMR analysis (Fig. S1–S4 and Table S1†), approximately 95% of free PLL and 50% of free GC were detected in a GCPLL colloidal solution in DMEM cell culture medium. For this reason, we hypothesised that most of the cytotoxic effect of the GCPLL MLWV solution might be associated with free GC molecules. In order to prove this hypothesis, GCPLL MLWVs were prepared as usual but fol-

lowed by a centrifugation step at 3000g for 5 minutes. The supernatant was discarded to eliminate the free forms of GC and PLL, and fresh DMEM culture medium was added. In order to ensure that the colloidal stability was maintained and aggregation diminished, we vortexed and sonicated the solution for a few seconds. Zeta-potential measurements of GCPLL MLWVs in cell culture medium, with a value of  $-11.9 \pm 0.4$  mV, confirmed a slight negative surface charge with positive outcomes in preventing aggregation.<sup>19,40,41</sup> Finally, as shown in Fig. 2b, L929 viability after incubation with centrifuged GCPLL MLWVs showed no significant cytotoxicity up to 122  $\mu\text{g mL}^{-1}$  compared to the 50% decrease shown when free GC was not removed.

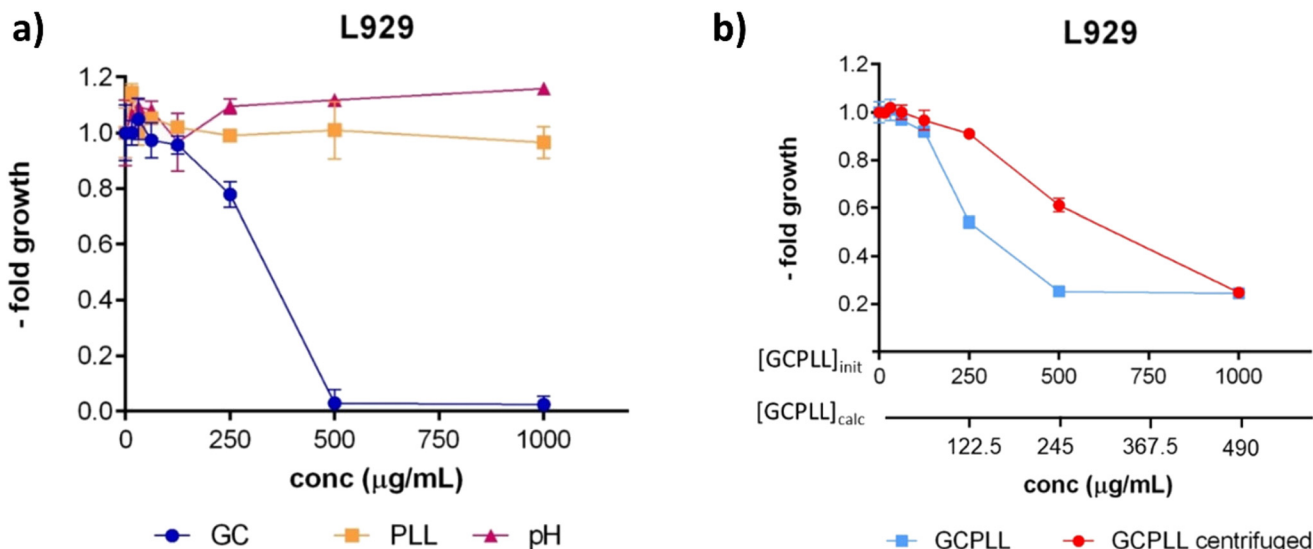
### 3.3. Curcumin is efficiently encapsulated within GCPLL MLWVs

The multilamellar lipid structure of GCPLL MLWVs, their stability in physiological culture medium and the absence of cytotoxicity make these self-assembled bodies interesting candidates as phospholipid-free drug delivery systems.

Curcumin (*Cur*), the active component of *Curcuma longa* plant, is a molecule widely used as a drug due to its antioxidant, anti-inflammatory and anticancer properties.<sup>42,43</sup> It is highly lipophilic, with a water-octanol partition coefficient ( $\log P$ ) in the order of 2.6 and a membrane partition constant above 10<sup>4</sup> M<sup>-1</sup>.<sup>44</sup> Similar to other hydrophobic drugs,<sup>45</sup> *Cur* has limited applicability due to its poor oral bioavailability, low chemical stability<sup>46</sup> and weak cellular uptake.<sup>42</sup> As a consequence, the accumulation of *Cur* is low within the cytoplasm as it interacts with the lipids of the cell membrane through H-bonding and hydrophobic interactions.<sup>47,48</sup> Different strategies were proposed in order to overcome these limitations such as the synthesis and use of curcumin derivatives<sup>42</sup> or the development of drug delivery systems which enhance its stability and increase its cellular uptake.<sup>49</sup> For this reason, we chose *Cur* as a model drug to load into the GCPLL MLWV system, with the aim of proving the encapsulation capability of the vesicles and to show their potential to enhance the therapeutic index of the encapsulated drug.

The zeta potential measured on GCPLL-*Cur* MLWVs, the loaded vesicles, exhibited a value of  $-13.2 \pm 0.3$  mV. The latter was not significantly different from the values measured for unloaded systems ( $-11.9 \pm 0.4$  mV). These results are in line with the preservation of the colloidal stability after resuspension. UV-visible absorbance measurements were performed to quantify the *Cur* encapsulated in GCPLL MLWVs just after





preparation and after 24 hours of incubation in culture medium. As shown in Fig. 3a, the absorption spectra were superimposable, thereby confirming that *Cur* was stable within the GCPLL MLWV solution over 24 hours and that it was encapsulated in its native form for concentrations up to 80  $\mu\text{M}$  (Fig. S5†). Considering that previous reports have shown that free *Cur* decomposes by approximately 50% in serum-supplemented cell culture media after 8 hours incubation, we consider these results as a critical advantage.

*Rhod* is a well-known fluorescence phospholipid label which intercalates into the glucolipid membrane without interfering with the structure when the lipid-to-dye molar ratio is above 200.<sup>50</sup> To confirm that *Cur* is actually colocalised in the GCPLL MLWVs and to exclude coprecipitation, we performed

fluorescence microscopy imaging on a drop of GCPLL-*Cur* MLWVs solution that was simultaneously labelled with *Rhod*. As seen in Fig. 3b, the colocalised fluorescence, red for *Rhod* and green for *Cur*, and differential interference contrast microscopy (DIC), white light for GCPLL MLWVs, confirmed the encapsulation of *Cur* within the GCPLL MLWVs.

A key parameter for the characterisation of drug delivery systems is the encapsulation efficiency (EE%), defined in (eqn (2)). EE% varies according to different properties related to each system such as morphology, hydrophobicity, surface charge, permeability, the structure of the encapsulated molecule, and the encapsulation process itself.<sup>51,52</sup> Considering the molar concentration of *Cur* to be 80  $\mu\text{M}$ , obtained by UV-VIS spectroscopy, and the total loaded *Cur* to be 135  $\mu\text{M}$ , EE% was

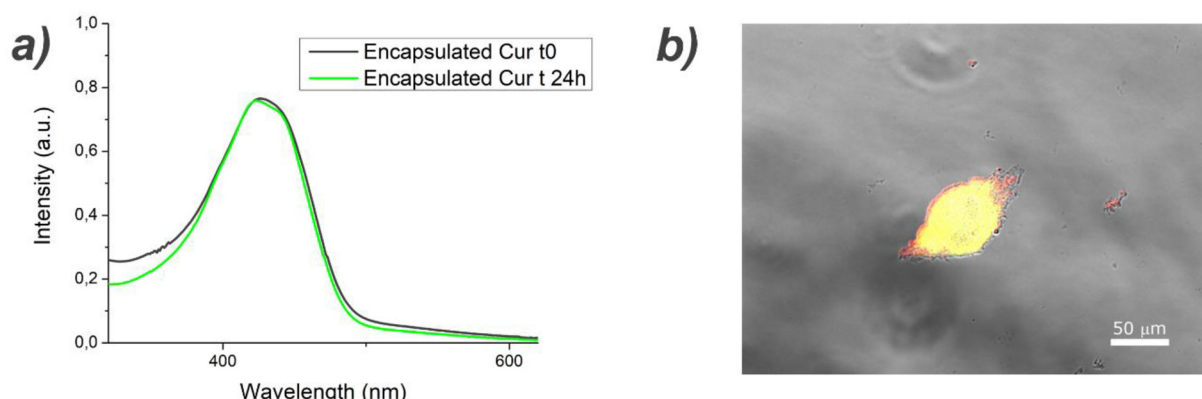


**Fig. 3** (a) UV-visible spectra of curcumin (*Cur*) encapsulated in GCPLL MLWVs at  $t = 0$  and  $t = 24$  h in DMEM cell culture medium. GCPLL-*Cur* MLWVs were centrifuged and resuspended in ethanol for analysis. (b) Fluorescence microscopy image of GCPLL-*Cur*-*Rhod* MLWVs at 2.5 mg  $\text{mL}^{-1}$  in DMEM cell culture medium. *Rhod* (red) and *Cur* (green) were loaded within the particles.



60%. This value was higher compared to other EE% values estimated for several vesicular systems, which show a high variability ranging from 1 to 68% for unilamellar vesicles (ULVs) and from 6 to 31% for multilamellar vesicles (MLVs).<sup>53</sup> The broad spectrum of reported EE% values between ULVs and MLVs is commonly explained by the presence of a lumen in ULVs, which accommodates a higher drug loading volume compared to the actual lipid content.<sup>53</sup> Despite the structural differences, we obtained EE% values comparable for both MLVs and ULVs. Another important parameter is the loading capacity (LC%), defined in (eqn (1)). LC% is defined as the ratio between the amount of encapsulated *Cur*, which was 30 µg, and the weight of GCPPL MLWVs calculated by <sup>1</sup>H solution NMR, which was 1225 µg. We obtained a LC% value for the GCPPL-*Cur* MLWV system of approximately 2.5%. Here, we hypothesise that the two-step preparation protocol for GCPPL-*Cur* MLWVs might explain the low values obtained for LC%. Considering that GCPPL MLWVs were already formed when *Cur* was added, encapsulation might occur only in the outer layers of the system. The strong discrepancy between LC% and EE% values might confirm this, indicating an optimal encapsulation process but a low drug-to-lipid content. While other protocols might improve both the EE% and LC% of this system, their study is out of the scope of the present work.

### 3.4. GCPPL MLWVs can be used to deliver curcumin to human cells

The biological activity of GCPPL-*Cur* MLWVs was explored using three different human cell lines, as shown in Fig. 4a–c. HeLa cells were chosen as a cancer model with high proliferation, NHDF cells were chosen as a model with moderate proliferation and THP-1-derived macrophages were used as non-dividing cells. Also, macrophages are members of the RES characterised by their high phagocytic activity, which helps to clear particles from the human body. Hence, the MLWV uptake by macrophages could be related to the persistence of particles in blood.

The cytotoxic effect of free *Cur* was explored on each kind of cell as a control experiment. As shown in Fig. 4d, the toxicity of free *Cur* was negligible for both THP-1-derived macrophages and NHDFs. However, there was a slight statistically relevant reduction in the viability of HeLa cells when the concentration of *Cur* was 5 µg mL<sup>-1</sup>, which decreased down to 75% of metabolic activity measured for control samples. The cytotoxic effect of GCPPL MLWVs was negligible for both NHDF and THP-1-derived macrophages, as seen in Fig. 4b and c. Therefore, only a slight decrease in cell viability was observed for HeLa cells at the highest concentration tested. As shown in Fig. 4a, for a concentration of 122 µg mL<sup>-1</sup> of GCPPL MLWVs, HeLa cell viability remained higher than 80% and therefore, no significant toxicity was observed.

GCPPL-*Cur* MLWVs showed a different behaviour. Fig. 4c shows that for loaded vesicles at concentrations up to 122 µg mL<sup>-1</sup> there was no significant effect on the viability of THP-1-derived macrophages. Additionally, NHDF metabolic activity decreased down to 75% when the concentration of GCPPL-*Cur*

MLWVs reached 122 µg mL<sup>-1</sup>. In contrast, the effect of GCPPL MLWVs on cancerous HeLa cells was dramatically different. Fig. 4a showed a drastic decrease to about 50% in cell viability for a concentration of 122 µg mL<sup>-1</sup>. Moreover, the cytotoxic effect of GCPPL-*Cur* MLWV was higher than that of free *Cur* despite a lower amount of carrier. For a calculated 3 µg mL<sup>-1</sup> *Cur* content in the most toxic GCPPL-*Cur* MLWV sample, there was approximately 50% cell viability, while for 5 µg mL<sup>-1</sup> free *Cur* concentration, cell viability was approximately 75%. As the cytotoxic effect of *Cur* encapsulated within GCPPL MLWVs was greater for HeLa cells compared to NHDF and THP-1-derived macrophages, we hypothesise that the cytotoxic effect of *Cur* might be correlated with cell doubling time.

Other studies reported a half-maximal inhibitory concentration (IC<sub>50</sub>) of 6.6 µM for carboxymethyl dextran (CMD)-modified liposomal *Cur* systems and IC<sub>50</sub> values of 21 µM and 16 µM for *Cur*-loaded cationic liposomes using HeLa and SiHa cells, respectively, and are comparable to ours.<sup>54,55</sup> These results evidence the remarkable activity of the GCPPL-*Cur* MLWV system towards cancerous HeLa cells. Moreover, with negligible cytotoxic effects on NHDF and non-dividing THP-1-derived macrophages, we hypothesise that this system might potentially avoid damage to normal tissues and the foreign particle elimination pathway through RES clearance.

Lipid-based particles can be taken up by cells following different cellular mechanisms, *i.e.* nanoparticles ranging from 50 to 100 nm can be engulfed by endocytosis, those less than 400 nm by micropinocytosis, and micrometric particles can enter the cells by phagocytosis.<sup>56,57</sup> Considering that the present GCPPL MLWV population is polydisperse, of diameter ranging from 50 nm to 10 µm,<sup>14</sup> we hypothesise that internalisation might not be the most appropriate route for drug delivery. For example, macrophages are prone to engulf particles ranging from 1 to 5 µm by phagocytosis, but particles were not observed within THP1 cells. In addition, cytotoxicity of curcumin encapsulated within GCPPL MLWVs seems to be correlated to the proliferative rate of cells.

We designed here proof-of-concept experiments to explore the release mechanism of *Cur* to the HeLa cell cytoplasm using GCPPL-*Cur* MLWVs and to better understand their cytotoxicity. As shown in Fig. 5a, *Cur* is confined within the cell cytoplasm, as observed by the green fluorescence signal surrounding the cell nucleus. The presence of *Cur* within the cytoplasm of HeLa cells can be further observed in Fig. S6 and S7,<sup>†</sup> which put in evidence the presence of green fluorescence grains only when HeLa cells were treated with GCPPL-*Cur* MLWVs. Moreover, the colocalization of *Cur* and *Rhod* in areas close to the cell membrane was evident, as observed in the yellow area on the merged image in Fig. 5a. However, in order to further understand if vesicles were either internalised or retained within the cell membrane of HeLa cells, we performed confocal microscopy imaging. As shown in Fig. 5b, HeLa cells treated with GCPPL-*Cur*-*Rhod* MLWVs clearly showed that GCPPL MLWVs, labelled in red with *Rhod*, are localised in the outer part of the cell membrane, while green areas corresponding to *Cur* are confined to the cytoplasm, sur-



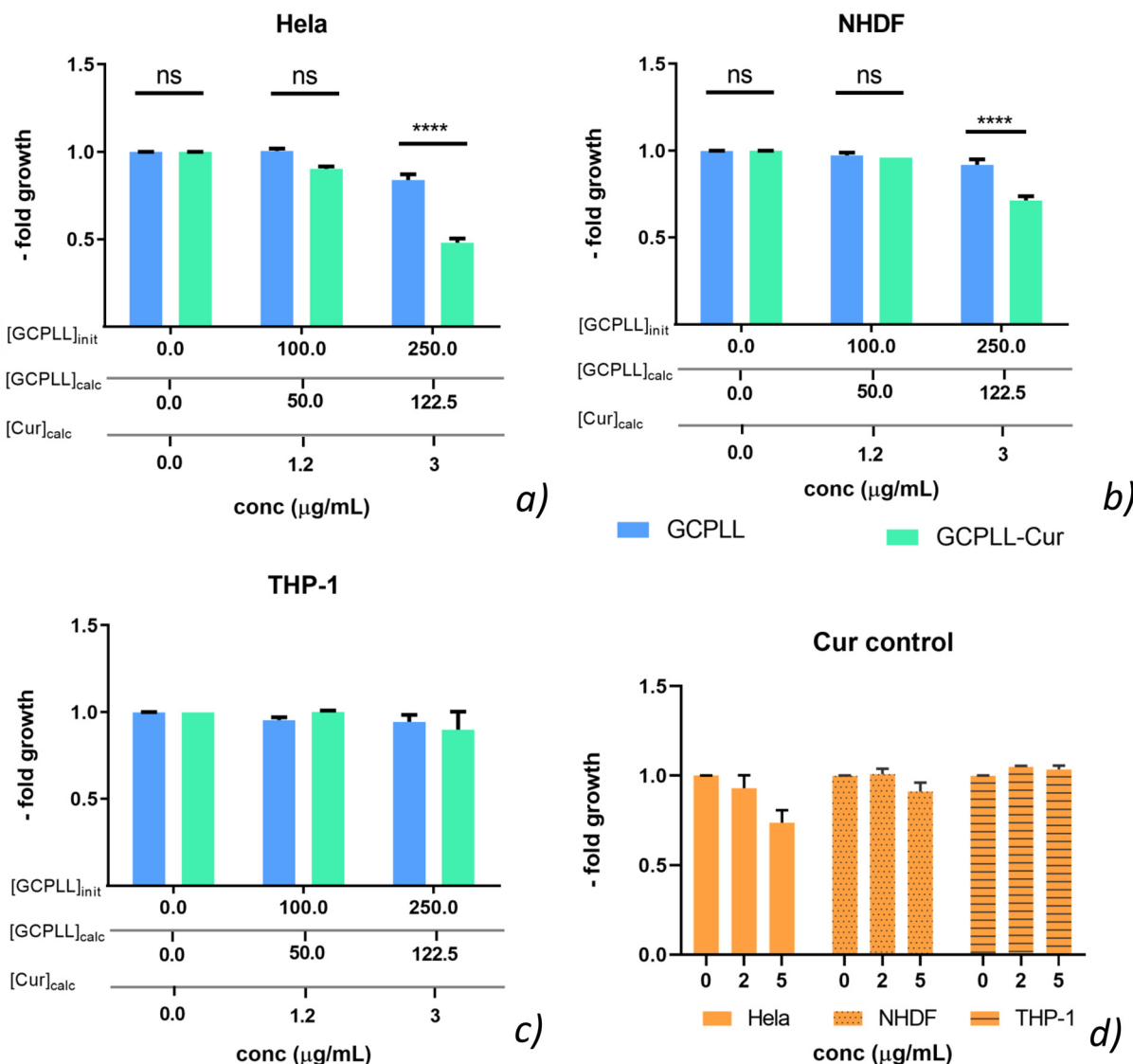


**Fig. 4** (a–c) Cell viability of GCPLL MLWVs (blue) and GCPLL-Cur MLWVs (green) in (a) HeLa cells; (b) NHDF cells, and (c) THP-1-derived macrophages. Three abscissas are displayed to show the initial concentration employed in the preparation of the vesicles, the calculated GCPLL content and the *Cur* encapsulated. In particular,  $[GCPLL]_{init}$  refers to the initial concentration employed in the preparation of GCPLL MLWVs,  $[GCPLL]_{calc}$  refers to the concentrations calculated by  $^1\text{H}$  solution NMR (Table 1) after centrifugation and resuspension of the GCPLL MLWV pellet, and  $[Cur]_{calc}$  refers to the encapsulated *Cur* in the GCPLL MLWVs measured by UV-Vis (Fig. 3). (d) Cell viability of free *Cur* control in the three different cell types tested. Results are presented as mean  $\pm$  SEM ( $n = 3$ , \*:  $p < 0.05$ , Kruskal–Wallis test).

rounding the cell nucleus. A schematic representation of the uptake mechanism is illustrated in Fig. 5c. As no red fluorescence signal was detected inside the HeLa cells, we understand that the delivery mechanism might not be governed by internalisation. Instead, we propose that GCPLL MLWVs might fuse or intertwine with the cell membrane to deliver *Cur* to the cell cytoplasm. However, further experimentation should be performed to corroborate these hypotheses.

Additionally, we also studied the interaction of the GCPLL MLWVs with NHDF and non-dividing THP-1 cells. As shown in Fig. 6a, green fluorescence grains are only observed within HeLa cells when the lamellar system is loaded with *Cur*. Flow cytometry measurements on the three cell lines tested, shown

in Fig. 6b, reveal differences in the uptake of GCPLL MLWVs. Dividing cells (HeLa cells and NHDF) showed the highest percentage of the *Rhod* label (around 40% using GCPLL-Cur *Rhod* MLWVs), compared to THP-1 cells (15% using GCPLL-Cur *Rhod* MLWVs). However, the detection of large quantities of curcumin within cells was only observed for HeLa cells.

### 3.5. GCPLL MLWVs can efficiently deliver chemotherapeutic compounds

The encouraging results showing the cytotoxicity of curcumin-loaded GCPLL MLWV against HeLa cells motivated further work to explore the possibility of employing this system for drug delivery. We then assessed the encapsulation feasibility



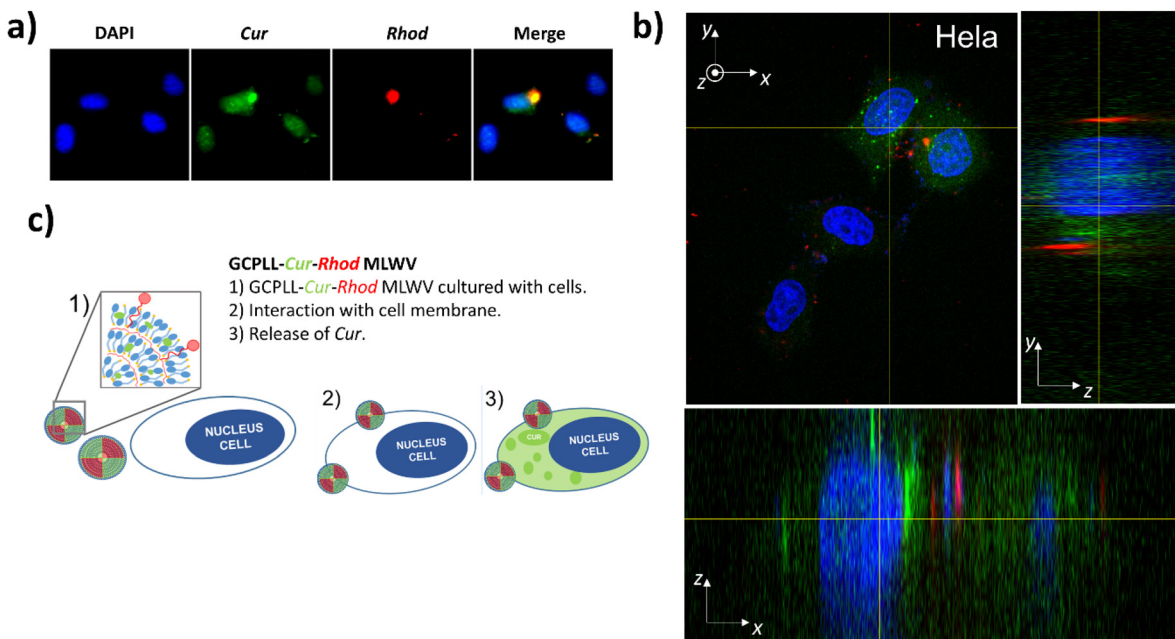


**Fig. 5** (a) Fluorescence confocal microscopy images of HeLa cells treated with  $100 \mu\text{g mL}^{-1}$  of GCPLL-Cur-Rhod MLWVs. (b) Orthogonal views obtained by confocal microscopy of HeLa cells treated with  $100 \mu\text{g mL}^{-1}$  GCPLL-Cur-Rhod MLWVs. The blue channel corresponds to the cell nucleus stained with DAPI, the green channel corresponds to Cur, and the red channel corresponds to GCPLL MLWVs stained with Rhod. (c) Schematic representation of the cellular uptake mechanism of GCPLL-Cur-Rhod MLWVs.

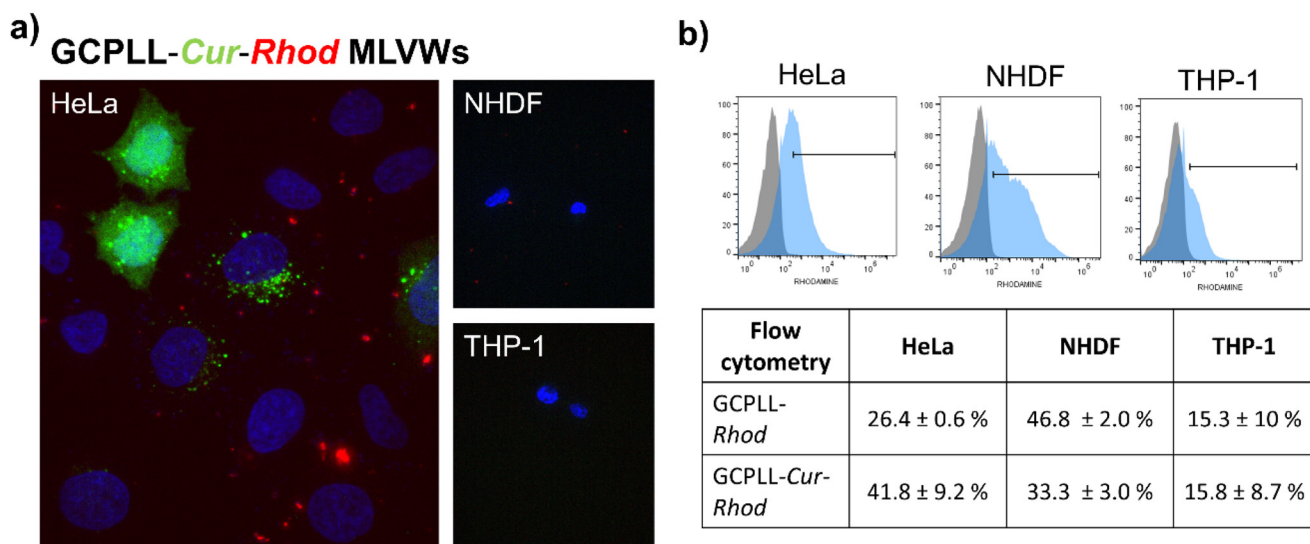


**Fig. 6** (a) Fluorescence microscopy images of HeLa, NHDF and THP-1 cells treated with  $100 \mu\text{g mL}^{-1}$  GCPLL-Cur-Rhod. The blue channel corresponds to the cell nucleus stained with DAPI, the green channel corresponds to Cur, and the red channel corresponds to GCPLL MLWVs stained with Rhod. (b) Flow cytometry FACS data of HeLa, NHDF and THP-1 cells incubated with  $100 \mu\text{g mL}^{-1}$  GCPLL-Rhod and GCPLL-Cur-Rhod MLWVs. Quantitative results show mean  $\pm$  SD values of triplicates for each cell line tested.

and toxicity of GCPLL MLWVs using a wider variety of chemotherapeutic compounds with different degrees of hydrophobicity. For instance, we tested these properties using standard anticancer drugs, namely doxorubicin (DOX,  $\log P = 1.41$ ),<sup>58</sup> paclitaxel (PAC,  $\log P = 3$ ),<sup>59</sup> and docetaxel (DOC,  $\log P = 2.4$ )<sup>60</sup>, on HeLa and NHDF cells. Using GCPLL-DOX MLWVs at  $122 \mu\text{g}$

$\text{mL}^{-1}$ , there was a decrease in HeLa cell viability, accounting for only  $26.8 \pm 1.7\%$  viable cells, when compared to empty GCPLL MLWVs, with  $89.5 \pm 3\%$  viable cells (Table 2). Regarding NHDF, cell viability decreased down to  $69.3 \pm 0.9\%$  when DOX-loaded vesicles were used. In comparison, unloaded vesicles did not impact cell viability. For GCPLL-PAC

**Table 2** Cell viability data from doxorubicin (DOX), paclitaxel (PAC) and docetaxel (DOC) delivery experiments tested on HeLa cells and NHDF cells, treated with prepared concentrations of  $100 \mu\text{g mL}^{-1}$  ( $50 \mu\text{g mL}^{-1}$ ) and  $250 \mu\text{g mL}^{-1}$  ( $125 \mu\text{g mL}^{-1}$ ) of GCPLL MLWVs. Results are expressed as mean  $\pm$  SEM ( $n = 3$ )

Cell viability $\pm$ SEM (%)	HeLa cells		NHDF cells	
	$100 \mu\text{g mL}^{-1}$	$250 \mu\text{g mL}^{-1}$	$100 \mu\text{g mL}^{-1}$	$250 \mu\text{g mL}^{-1}$
GCPLL	$93.3 \pm 6.9$	$89.5 \pm 3.0$	$95.9 \pm 2.9$	$98.7 \pm 1.3$
GCPLL-DOX	$66.9 \pm 1.8$	$26.8 \pm 1.7$	$81.3 \pm 1.4$	$69.3 \pm 0.9$
GCPLL-PAC	$98.7 \pm 1.2$	$59.3 \pm 0.6$	$91.6 \pm 5.6$	$77.7 \pm 6.2$
GCPLL-DOC	$79.5 \pm 8.1$	$44.3 \pm 1.3$	$85.5 \pm 4.2$	$67.0 \pm 2.0$

and GCPLL-DOC treatments at  $122 \mu\text{g mL}^{-1}$ , both loaded systems showed a cell viability higher than 65% for NHDF. However, when HeLa cells were treated, the cytotoxic effect was observed with a cell viability measured at  $59.3 \pm 0.6\%$  and  $44.3 \pm 1.3\%$ , respectively. Both PAC- and DOC-loaded systems exhibited a lower cytotoxicity compared with that obtained with DOX.

## 4. Conclusions

This study demonstrates that microbial glycolipid amphiphiles with the ability to assemble into membranes can be used to prepare colloidal drug carriers in the absence of a phospholipid-based scaffold. Multilamellar wall vesicle (MLWV) colloids were prepared from a monounsaturated single-glucose lipid (GC) complexed with poly-L-lysine (PLL), a biocompatible poly-electrolyte. MLWVs are stable at physiological pH in cell culture medium. Curcumin (*Cur*), a natural lipophilic drug model, was efficiently (60%) encapsulated in the MLWVs, which show a greater therapeutic effect compared to free *Cur* treatments. The vesicles interact more efficiently with dividing cells (HeLa and NHDF) than with non-dividing ones (macrophages). In addition, the cytotoxic effect of curcumin is specific to cancerous HeLa cells because the viability of fibroblasts and macrophages is not affected by *Cur*-loaded MLWVs. This suggests that *Cur*-loaded systems may increase the circulation time of lipophilic drugs in the bloodstream when they are confined within the MLWVs, thereby potentially reducing unwanted cytotoxic side effects. Lastly, GCPLL MLWVs are able to efficiently deliver other chemotherapeutic drugs (doxorubicin, paclitaxel and docetaxel). This work shows that microbial glycolipid amphiphiles can be used as stand-alone soft drug carriers. It is believed that the pH responsivity of this class of molecules is a property that can be exploited in future work to develop pH-responsive glycolipid carriers.

## Author contributions

S. A. dC., C. H. and N. B. contributed to the design of the study. S. A. dC., C. S., K. O., J. D., L. R. and J. P. conducted

experiments and data analysis. S. A. dC., J. D., L. R., J. P., C. H. and N. B. provided technical advice and interpretation of results. S. A. dC., C. H., N. B. and S. O. F. wrote the manuscript and ESI.† All the authors commented on and amended both documents. All the authors discussed and contributed to the work.

## Data availability

Data for this article, including graphs and images, are available at Zenodo at <https://doi.org/10.5281/zenodo.13625001>.

## Conflicts of interest

There are no conflicts of interest to declare.

## Acknowledgements

This work was supported by French state funds managed by the Agence Nationale de la Recherche (ANR) within the Investissements d'Avenir program under reference ANR-11-IDEX-0004-02 and more specifically within the framework of the Cluster of Excellence MATISSE. ANR also supported this project within the framework of SELFAMPHI 19-CE43-0012-01.

## References

- 1 J. D. Desai and I. M. Banat, Microbial production of surfactants and their commercial potential, *Microbiol. Mol. Biol. Rev.*, 1997, **61**(1), 47–64, DOI: [10.1128/mmbr.61.1.47-64.1997](https://doi.org/10.1128/mmbr.61.1.47-64.1997).
- 2 L. R. Rodrigues, L. R. Rodrigues and J. A. Teixeira, Biomedical and Therapeutic Applications of A Biosurfactants, *Adv. Exp. Med. Biol.*, 2010, **672**, 75–87.
- 3 F. Haque, M. S. A. Khan and N. AlQurashi, ROS-Mediated Necrosis by Glycolipid Biosurfactants on Lung, Breast, and Skin Melanoma Cells, *Front. Oncol.*, 2021, **11**, 1–13, DOI: [10.3389/fonc.2021.622470](https://doi.org/10.3389/fonc.2021.622470).
- 4 P. Thakur, N. K. Saini, V. K. Thakur, V. K. Gupta, R. V. Saini and A. K. Saini, Rhamnolipid the Glycolipid Biosurfactant: Emerging trends and promising strategies in the field of biotechnology and biomedicine, *Microb. Cell Fact.*, 2021, **20**(1), 1–15, DOI: [10.1186/s12934-020-01497-9](https://doi.org/10.1186/s12934-020-01497-9).
- 5 S. L. Fu, S. R. Wallner, W. B. Bowne, *et al.*, Sophorolipids and Their Derivatives Are Lethal Against Human Pancreatic Cancer Cells, *J. Surg. Res.*, 2008, **148**(1), 77–82, DOI: [10.1016/j.jss.2008.03.005](https://doi.org/10.1016/j.jss.2008.03.005).
- 6 B. Callaghan, H. Lydon, S. L. K. W. Roelants, *et al.*, Lactonic sophorolipids increase tumor burden in Apcmin $^{+/-}$  mice, *PLoS One*, 2016, **11**(6), e0156845, DOI: [10.1371/journal.pone.0156845](https://doi.org/10.1371/journal.pone.0156845).
- 7 L. R. Rodrigues, Microbial surfactants: Fundamentals and applicability in the formulation of nano-sized drug delivery



vectors, *J. Colloid Interface Sci.*, 2015, **449**, 304–316, DOI: [10.1016/j.jcis.2015.01.022](https://doi.org/10.1016/j.jcis.2015.01.022).

8 M. Nakanishi, Y. Inoh, D. Kitamoto and T. Furuno, Nano vectors with a biosurfactant for gene transfection and drug delivery, *J. Drug Delivery Sci. Technol.*, 2009, **19**(3), 165–169, DOI: [10.1016/S1773-2247\(09\)50031-7](https://doi.org/10.1016/S1773-2247(09)50031-7).

9 B. C. P. Sanches, C. A. Rocha, J. G. M. Bedoya, *et al.*, Rhamnolipid-based liposomes as promising nano-carriers for enhancing the antibacterial activity of peptides derived from bacterial toxin-antitoxin systems, *Int. J. Nanomed.*, 2021, **16**, 925–939, DOI: [10.2147/IJN.S283400](https://doi.org/10.2147/IJN.S283400).

10 A. Ortiz, J. A. Teruel, M. J. Espuny, A. Marqués, Á. Manresa and F. J. Aranda, Interactions of a bacterial biosurfactant trehalose lipid with phosphatidylserine membranes, *Chem. Phys. Lipids*, 2009, **158**(1), 46–53, DOI: [10.1016/j.chemphyslip.2008.11.001](https://doi.org/10.1016/j.chemphyslip.2008.11.001).

11 A. Ortiz, J. A. Teruel, Á. Manresa, M. J. Espuny, A. Marqués and F. J. Aranda, Effects of a bacterial trehalose lipid on phosphatidylglycerol membranes, *Biochim. Biophys. Acta, Biomembr.*, 2011, **1808**(8), 2067–2072, DOI: [10.1016/j.bbamem.2011.05.003](https://doi.org/10.1016/j.bbamem.2011.05.003).

12 D. E. Otzen, Biosurfactants and surfactants interacting with membranes and proteins: Same but different?, *Biochim. Biophys. Acta, Biomembr.*, 2017, **1859**(4), 639–649, DOI: [10.1016/j.bbamem.2016.09.024](https://doi.org/10.1016/j.bbamem.2016.09.024).

13 F. Müller, S. Hönzke, W. O. Luthardt, *et al.*, Rhamnolipids form drug-loaded nanoparticles for dermal drug delivery, *Eur. J. Pharm. Biopharm.*, 2017, **116**, 31–37, DOI: [10.1016/j.ejpb.2016.12.013](https://doi.org/10.1016/j.ejpb.2016.12.013).

14 N. Baccile, M. Selmane, P. Le Griel, *et al.*, PH-Driven Self-Assembly of Acidic Microbial Glycolipids, *Langmuir*, 2016, **32**(25), 6343–6359, DOI: [10.1021/acs.langmuir.6b00488](https://doi.org/10.1021/acs.langmuir.6b00488).

15 N. Baccile, C. Seyrig, A. Poirier, S. Alonso-De Castro, S. L. K. W. Roelants and S. Abel, Self-assembly, interfacial properties, interactions with macromolecules and molecular modelling and simulation of microbial bio-based amphiphiles (biosurfactants). A tutorial review, *Green Chem.*, 2021, **23**(11), 3842–3944, DOI: [10.1039/d1gc00097g](https://doi.org/10.1039/d1gc00097g).

16 C. R. Safinya, Structures of lipid-DNA complexes: Supramolecular assembly and gene delivery, *Curr. Opin. Struct. Biol.*, 2001, **11**(4), 440–448, DOI: [10.1016/S0959-440X\(00\)00230-X](https://doi.org/10.1016/S0959-440X(00)00230-X).

17 N. Baccile, A. Poirier, C. Seyrig, *et al.*, Chameleonic amphiphile: The unique multiple self-assembly properties of a natural glycolipid in excess of water, *J. Colloid Interface Sci.*, 2023, **630**, 404–415, DOI: [10.1016/j.jcis.2022.07.130](https://doi.org/10.1016/j.jcis.2022.07.130).

18 C. Seyrig, G. Kignelman, W. Thielemans, *et al.*, Stimuli-Induced Nonequilibrium Phase Transitions in Polyelectrolyte-Surfactant Complex Coacervates, *Langmuir*, 2020, **36**(30), 8839–8857, DOI: [10.1021/acs.langmuir.0c01177](https://doi.org/10.1021/acs.langmuir.0c01177).

19 C. Seyrig, P. Le Griel, N. Cowieson, J. Perez and N. Baccile, Synthesis of multilamellar walls vesicles polyelectrolyte-surfactant complexes from pH-stimulated phase transition using microbial biosurfactants, *J. Colloid Interface Sci.*, 2020, **580**, 493–502, DOI: [10.1016/j.jcis.2020.07.021](https://doi.org/10.1016/j.jcis.2020.07.021).

20 J. Majumder and T. Minko, Multifunctional and stimuli-responsive nanocarriers for targeted therapeutic delivery, *Expert Opin. Drug Delivery*, 2021, **18**(2), 205–227, DOI: [10.4049/jimmunol.1801473.The](https://doi.org/10.4049/jimmunol.1801473.The).

21 S. P. Metkar, G. Fernandes, P. D. Navti, *et al.*, Nanoparticle drug delivery systems in hepatocellular carcinoma: A focus on targeting strategies and therapeutic applications, *OpenNano*, 2023, **12**, 100159, DOI: [10.1016/j.onano.2023.100159](https://doi.org/10.1016/j.onano.2023.100159).

22 N. Filipczak, J. Pan, S. S. K. Yalamarty and V. P. Torchilin, Recent advancements in liposome technology, *Adv. Drug Delivery Rev.*, 2020, **156**, 4–22, DOI: [10.1016/j.addr.2020.06.022](https://doi.org/10.1016/j.addr.2020.06.022).

23 J. Kopeček and J. Yang, Polymer nanomedicines, *Adv. Drug Delivery Rev.*, 2020, **156**, 40–64, DOI: [10.1016/j.addr.2020.07.020](https://doi.org/10.1016/j.addr.2020.07.020).

24 H. S. Patel, S. J. Shaikh, D. Ray, *et al.*, Structural transitions in mixed Phosphatidylcholine/Pluronic micellar systems and their in vitro therapeutic evaluation for poorly water-soluble drug, *J. Mol. Liq.*, 2022, **364**, 120003, DOI: [10.1016/j.molliq.2022.120003](https://doi.org/10.1016/j.molliq.2022.120003).

25 D. Hwang, J. D. Ramsey and A. V. Kabanov, Polymeric micelles for the delivery of poorly soluble drugs: From nanoformulation to clinical approval, *Adv. Drug Delivery Rev.*, 2020, **156**, 80–118, DOI: [10.1016/j.addr.2020.09.009](https://doi.org/10.1016/j.addr.2020.09.009).

26 A. Varanko, S. Saha and A. Chilkoti, Recent trends in protein and peptide-based biomaterials for advanced drug delivery, *Adv. Drug Delivery Rev.*, 2020, **156**, 133–187.

27 D. C. Luther, R. Huang, T. Jeon, *et al.*, Delivery of drugs, proteins, and nucleic acids using inorganic nanoparticles, *Adv. Drug Delivery Rev.*, 2020, **156**(2020), 188–213, DOI: [10.1016/j.addr.2020.06.020](https://doi.org/10.1016/j.addr.2020.06.020).

28 K. K. Jain, An Overview of Drug Delivery Systems, in *Methods in Molecular Biology 2059: Drug Delivery Systems*, 2011, pp. 1–54. DOI: [10.1201/b10846](https://doi.org/10.1201/b10846).

29 Z. Jamalpoor, H. Ahmadi, M. Heydari, M. Abdouss, A. Rahdar and A. M. Díez-Pascual, Chitosan based niosomal hydrogel with polyethylene glycol and halloysite nanotubes for curcumin delivery, *J. Mol. Liq.*, 2024, **401**, 124640, DOI: [10.1016/j.molliq.2024.124640](https://doi.org/10.1016/j.molliq.2024.124640).

30 L. Sercombe, T. Veerati, F. Moheimani, S. Y. Wu, A. K. Sood and S. Hua, Advances and challenges of liposome assisted drug delivery, *Front. Pharmacol.*, 2015, **6**(286), 1–13, DOI: [10.3389/fphar.2015.00286](https://doi.org/10.3389/fphar.2015.00286).

31 S. Senapati, A. K. Mahanta, S. Kumar and P. Maiti, Controlled drug delivery vehicles for cancer treatment and their performance, *Signal Transduction Targeted Ther.*, 2018, **3**(1), 1–19, DOI: [10.1038/s41392-017-0004-3](https://doi.org/10.1038/s41392-017-0004-3).

32 Q. Li, X. Li and C. Zhao, Strategies to Obtain Encapsulation and Controlled Release of Small Hydrophilic Molecules, *Front. Bioeng. Biotechnol.*, 2020, **8**, 1–6, DOI: [10.3389/fbioe.2020.00437](https://doi.org/10.3389/fbioe.2020.00437).

33 M. Pourmadadi, P. Abbasi, M. M. Eshaghi, *et al.*, Curcumin delivery and co-delivery based on nanomaterials as an effective approach for cancer therapy, *J. Drug Delivery Sci. Technol.*, 2022, **78**, 103982, DOI: [10.1016/j.jddst.2022.103982](https://doi.org/10.1016/j.jddst.2022.103982).



34 K. M. J. Saerens, J. Zhang, L. Saey, I. N. A. Van Bogaert and W. Soetaert, Cloning and functional characterization of the UDP-glucosyltransferase UgtB I involved in sophorolipid production by *Candida bambicola* and creation of a glucolipid-producing yeast strain, *Yeast*, 2011, **28**, 279–292, DOI: [10.1002/yea.10002](https://doi.org/10.1002/yea.10002).

35 A. I. Novaira, V. Avila, G. G. Montich and C. M. Previtali, Fluorescence quenching of anthracene by indole derivatives in phospholipid bilayers, *J. Photochem. Photobiol. B*, 2001, **60**(1), 25–31, DOI: [10.1016/S1011-1344\(01\)00112-9](https://doi.org/10.1016/S1011-1344(01)00112-9).

36 M. Leonard-Latour, R. M. Morelis and P. R. Coulet, Influence of pyrene-based fluorescent probes on the characteristics of DMPA/DMPC Langmuir-Blodgett films, *Langmuir*, 1996, **12**(20), 4797–4802, DOI: [10.1021/la960072x](https://doi.org/10.1021/la960072x).

37 U. Nandi, I. Onyesom and D. Douroumis, An in vitro evaluation of antitumor activity of sirolimus-encapsulated liposomes in breast cancer cells, *J. Pharm. Pharmacol.*, 2021, **73**(3), 300–309, DOI: [10.1093/jpp/rga0061](https://doi.org/10.1093/jpp/rga0061).

38 W. Wang, G. F. Shu, K. J. Lu, *et al.*, Flexible liposomal gel dual-loaded with all-trans retinoic acid and betamethasone for enhanced therapeutic efficiency of psoriasis, *J. Nanobiotechnol.*, 2020, **18**(1), 1–14, DOI: [10.1186/s12951-020-00635-0](https://doi.org/10.1186/s12951-020-00635-0).

39 T. Feng, Y. Wei, R. J. Lee and L. Zhao, Liposomal curcumin and its application in cancer Physical property, *Int. J. Nanomed.*, 2017, **12**, 6027–6044.

40 S. Patil, A. Sandberg, E. Heckert, W. Self and S. Seal, Protein adsorption and cellular uptake of cerium oxide nanoparticles as a function of zeta potential, *Biomaterials*, 2007, **28**(31), 4600–4607, DOI: [10.1016/j.biomaterials.2007.07.029](https://doi.org/10.1016/j.biomaterials.2007.07.029).

41 S. Puttipipatkhachorn, J. Nunthanid, K. Yamamoto and G. E. Peck, Drug physical state and drug-polymer interaction on drug release from chitosan matrix films, *J. Controlled Release*, 2001, **75**(1–2), 143–153, DOI: [10.1016/S0168-3659\(01\)00389-3](https://doi.org/10.1016/S0168-3659(01)00389-3).

42 M. A. Tomeh, R. Hadianamrei and X. Zhao, A review of curcumin and its derivatives as anticancer agents, *Int. J. Mol. Sci.*, 2019, **20**(5), 1033, DOI: [10.3390/ijms20051033](https://doi.org/10.3390/ijms20051033).

43 A. Goel, A. B. Kunnumakkara and B. B. Aggarwal, Curcumin as “Curecumin”: From kitchen to clinic, *Biochem. Pharmacol.*, 2008, **75**(4), 787–809, DOI: [10.1016/j.bcp.2007.08.016](https://doi.org/10.1016/j.bcp.2007.08.016).

44 M. Herger, G. R. Van, M. Broekgaarden and M. C. Michel, The Molecular Basis for the Pharmacokinetics and Pharmacodynamics of Curcumin and its Metabolites in Relation to Cancer, *Cancer Pharmacol. Rev.*, 2014, **66**, 222–307.

45 S. Kalepu and V. Nekkanti, Insoluble drug delivery strategies: Review of recent advances and business prospects, *Acta Pharm. Sin. B*, 2015, **5**(5), 442–453, DOI: [10.1016/j.apsb.2015.07.003](https://doi.org/10.1016/j.apsb.2015.07.003).

46 W. W. Quitschke, Differential solubility of curcuminoids in serum and albumin solutions: Implications for analytical and therapeutic applications, *BMC Biotechnol.*, 2008, **8**, 1–17, DOI: [10.1186/1472-6750-8-84](https://doi.org/10.1186/1472-6750-8-84).

47 J. Barry, M. Fritz, J. R. Brender, P. E. S. Smith, D. K. Lee and A. Ramamoorthy, Determining the effects of lipophilic drugs on membrane structure by solid-state NMR spectroscopy: The case of the antioxidant curcumin, *J. Am. Chem. Soc.*, 2009, **131**(12), 4490–4498, DOI: [10.1021/ja809217u](https://doi.org/10.1021/ja809217u).

48 M. Tsukamoto, K. Kuroda, A. Ramamoorthy and K. Yasuhara, Modulation of raft domains in a lipid bilayer by boundary-active curcumin, *Chem. Commun.*, 2014, **50**(26), 3427–3430, DOI: [10.4049/jimmunol.1801473.The](https://doi.org/10.4049/jimmunol.1801473.The).

49 A. Karthikeyan, N. Senthil and T. Min, Nanocurcumin: A Promising Candidate for Therapeutic Applications, *Front. Pharmacol.*, 2020, **11**, 1–24, DOI: [10.3389/fphar.2020.00487](https://doi.org/10.3389/fphar.2020.00487).

50 G. Ben Messaoud, P. Le Griel, S. Prévost, *et al.*, Single-molecule lamellar hydrogels from bolaform microbial glucolipids, *Soft Matter*, 2020, **16**(10), 2528–2539, DOI: [10.1039/c9sm02158b](https://doi.org/10.1039/c9sm02158b).

51 A. R. Nicholas, M. J. Scott, N. I. Kennedy and M. N. Jones, Effect of grafted polyethylene glycol (PEG) on the size, encapsulation efficiency and permeability of vesicles, *Biochim. Biophys. Acta, Biomembr.*, 2000, **1463**(1), 167–178, DOI: [10.1016/S0005-2736\(99\)00192-3](https://doi.org/10.1016/S0005-2736(99)00192-3).

52 S. Kulkarni, G. V. Betageri and M. Singh, Factors affecting microencapsulation of drugs in liposomes, *J. Microencapsulation*, 1995, **12**, 229–246.

53 B. Sun and D. T. Chiu, Determination of the encapsulation efficiency of individual vesicles using single-vesicle photolysis and confocal single-molecule detection, *Anal. Chem.*, 2005, **77**(9), 2770–2776, DOI: [10.1021/ac048439n](https://doi.org/10.1021/ac048439n).

54 Q. Huang, L. Zhang, X. Sun, K. Zeng, J. Li and Y. N. Liu, Coating of carboxymethyl dextran on liposomal curcumin to improve the anticancer activity, *RSC Adv.*, 2014, **4**(103), 59211–59217, DOI: [10.1039/c4ra11181h](https://doi.org/10.1039/c4ra11181h).

55 N. Saengkrit, S. Saesoo, W. Srinuanchai, S. Phunpee and U. R. Ruktanonchai, Influence of curcumin-loaded cationic liposome on anticancer activity for cervical cancer therapy, *Colloids Surf. B*, 2014, **114**, 349–356, DOI: [10.1016/j.colsurfb.2013.10.005](https://doi.org/10.1016/j.colsurfb.2013.10.005).

56 P. Foroozandeh and A. A. Aziz, Insight into Cellular Uptake and Intracellular Trafficking of Nanoparticles, *Nanoscale Res. Lett.*, 2018, **13**, 339, DOI: [10.1186/s11671-018-2728-6](https://doi.org/10.1186/s11671-018-2728-6).

57 D. Manzanares and V. Ceña, Endocytosis: The nanoparticle and submicron nanocompounds gateway into the cell, *Pharmaceutics*, 2020, **12**(4), 1–22, DOI: [10.3390/pharmaceutics12040371](https://doi.org/10.3390/pharmaceutics12040371).

58 Doxorubicin hydrochloride. DrugBank Online. (Accessed: 31st January 2024). Available at: <https://go.drugbank.com/salts/DBSALT000060>.

59 Paclitaxel: Uses, Interactions, Mechanisms of Action. DrugBank Online. (Accessed: 31st January 2024). Available at: <https://go.drugbank.com/drugs/DB01229>.

60 Docetaxel: Uses, Interactions, Mechanisms of Action. DrugBank Online. (Accessed: 31st January 2024). Available at: <https://go.drugbank.com/drugs/DB01248>.

